
Mirror Bridges Between Probability Measures

Leticia Mattos Da Silva

Massachusetts Institute of Technology
leticiam@mit.edu

Silvia Sellán

Massachusetts Institute of Technology
Columbia University
silviaseilan@cs.columbia.edu

Francisco Vargas

Cambridge University
Xaira Therapeutics
fav25@cam.ac.uk

Justin Solomon

Massachusetts Institute of Technology
jsolomon@mit.edu

Abstract

Resampling from a target measure whose density is unknown is a fundamental problem in mathematical statistics and machine learning. A setting that dominates the machine learning literature consists of learning a map from an easy-to-sample prior, such as the Gaussian distribution, to a target measure. Under this model, samples from the prior are pushed forward to generate a new sample on the target measure, which is often difficult to sample from directly. Of particular interest is the problem of generating a new sample that is proximate to or otherwise conditioned on a given input sample. In this paper, we propose a new model called *mirror bridges* to solve this problem of conditional resampling. Our key observation is that solving the Schrödinger bridge problem between a distribution and itself provides a natural way to produce new samples from conditional distributions, giving in-distribution variations of an input data point. We demonstrate how to efficiently estimate the solution to this largely overlooked version of the Schrödinger bridge problem, and we prove that under mild conditions, the difference between our estimate and the true Schrödinger bridge can be controlled explicitly. We show that our proposed method leads to significant algorithmic simplifications over existing alternatives, in addition to providing control over in-distribution variation. Empirically, we demonstrate how these benefits can be leveraged to produce proximal samples in a number of application domains.

1 Introduction

Mapping one probability distribution to another is a central technique in mathematical statistics and machine learning. Myriad computational tools have been proposed for this critical yet often challenging task. Models and techniques for optimal transport provide one class of examples, where methods like the Hungarian algorithm [Kuhn, 1955] map one distribution to another with optimal cost. Adding entropic regularization to the static optimal transport problem yields efficient algorithms like Sinkhorn’s method [Deming and Stephan, 1940, Sinkhorn, 1964], which have been widely adopted in machine learning since their introduction by Cuturi [2013]. Static entropy-regularized optimal transportation is equivalent to a dynamical formulation known as the *Schrödinger bridge problem* [Schrödinger, 1932, Léonard, 2014], which has proven useful to efficiently compute an approximation of the optimal map paired with an interpolant between the input measures.

Inspired by these mathematical constructions and efficient optimization algorithms, several methods in machine learning rely on learning a map from one distribution to another. Beyond optimal transport, diffusion models, for instance, learn to reverse a diffusion process that maps data to a noisy prior.

Our method allows resampling with control over in-distribution variation

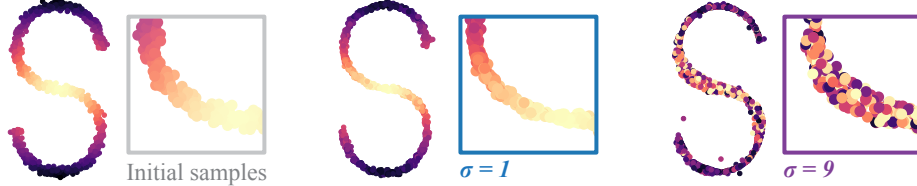


Figure 1: We visualize the resampling of a 2D distribution obtained with our method for different values of noise σ . Higher noise value results in greater in-distribution sample variance.

Special attention has been given to learning methods that accomplish this in a *stochastic* manner, i.e., modeling the forward noising process using a stochastic differential equation (SDE).

The most common learning applications of distribution mapping attempt to find a map from a simple prior distribution to a complex data distribution, either using a score-matching strategy [Song and Ermon, 2019, Ho et al., 2020, Song et al., 2021] or leveraging a formulation of the Schrödinger bridge problem [De Bortoli et al., 2021, Shi et al., 2022, 2023, Zhou et al., 2024]; other learning applications map one complex data distribution to another [Cuturi, 2013, Courty et al., 2017].

Rather than mapping a simple prior to a complex data distribution, in this paper we instead tackle the understudied problem of mapping a probability distribution to *itself*, that is, finding a joint distribution whose marginals are both the same data distribution π . This task might seem inane at first glance, since two simple couplings satisfy our constraints: one is the independent coupling $p(x, y) = \pi(x)\pi(y)$, and the other is the “diagonal” map given by $p(x, y) = \pi(x)\delta_y$. The space of couplings between a measure and itself, however, is far richer than these two extremes and includes models whose conditional distributions are neither identical nor Dirac measures.

We focus on the class of self-maps obtained by entropy-regularized transport from a measure to itself. Formally, we define a *mirror Schrödinger bridge* to be the minimizer of the KL divergence $D_{\text{KL}}(\mathbb{P} \parallel \mathbb{P}^0)$ over path measures \mathbb{P} with both initial and final marginal distributions equal to π , where \mathbb{P}^0 is an Ornstein-Uhlenbeck process with noise σ . Mirror Schrödinger bridges are the stochastic counterpart to minimizing $D_{\text{KL}}(p \parallel p^0)$, where p^0 is the probability density of the joint distribution associated with the path measure \mathbb{P}^0 , over the joint distributions p on $\mathbb{R}^n \times \mathbb{R}^n$ satisfying the linear constraints $\int p(x, y)dy = \pi(x)$ and $\int p(x, y)dx = \pi(y)$. While the former minimizes the Kullback-Leibler divergence on path space, the latter is a minimization over density couplings.

Despite its simplicity, the mirror case of the Schrödinger bridge problem suggests a rich application space. Couplings with identical marginals have proven useful to enhance model accuracy in vision and natural language processing by reinterpreting attention matrices as transport plans [Sander et al., 2022]. Few works, however, consider this task from the perspective of optimizing over path measures or provide control over the entropy of the matching at test time. Albergo et al. [2023] propose a stochastic interpolant between a distribution and itself, but their interpolants are not minimal in the relative entropy sense. Such minimal interpolants are those with minimal kinetic energy, and in applications, minimizing the kinetic energy of a path has been correlated to faster sampling [Shaul et al., 2023].

Contributions. We investigate the mirror Schrödinger bridge problem and demonstrate how it can be leveraged to obtain in-distribution variants of a given input sample. In particular, given a sample $x_0 \sim p_{\text{data}}$, we build an estimate for the stochastic process $\{\mathbf{X}_t\}_{t \in [0, 1]}$ with minimal relative entropy under which the sample x_0 arrives at some $x_1 \sim p_{\text{data}}$ with x_1 proximal but not identical to x_0 . We call our estimate a *mirror bridge*. Although this estimate might not be the mirror Schrödinger bridge, we prove that under mild conditions the former is a good approximation of the latter in an explicitly quantifiable way. Furthermore, we demonstrate that our algorithm for obtaining mirror bridges has computational advantages over alternatives used to compute Schrödinger bridges.

Our contributions are twofold. First, on the theoretical side, we use the time symmetry of the mirror Schrödinger bridge to express it as the limit of iterates produced by a symmetrized version of the Iterative Proportional Fitting Procedure (IPFP). We show that this scheme admits a convenient first-order approximation in terms of a convergent alternating minimization procedure that dramatically reduces computational expense in practice. Our mirror bridge is the limit of the latter procedure, and we provide an error bound to justify it as a good approximation. Second, in applications, the implementation of our method allows for sampling from the conditional distribution $\mathbf{X}_1 \mid \mathbf{X}_0 = x_0$, allowing us to control how proximal a generated sample x_1 is relative to the input sample x_0 .

2 Related Works

Entropy regularized optimal transport. A few recent works employ the idea of a coupling with the same marginal constraints. Feydy et al. [2019], Mensch et al. [2019] use static entropy-regularized optimal transportation from a distribution to itself to build a cost function correlated to uncertainty. Sander et al. [2022] reinterpret attention matrices in transformers as transport plans from a distribution to itself, while Agarwal et al. [2024] analyze this reinterpretation in the context of gradient flows. Also relevant is the work of Kurras [2015], who shows that, over discrete state spaces, Sinkhorn’s algorithm can be simplified in the case of identical marginal constraints. These works do not consider the coupling with the same marginal constraints from the perspective of path measures on continuous-state spaces. In our paper, we focus on the path measure formulation instead of viewing it as a self-transport map and present a practical algorithm to solve it.

Expectation maximization. Our method can be categorized under the umbrella of expectation maximization algorithms, drawing from the theory of information geometry. A number of recent papers introduce related formulations to machine learning; most relevant to us are Brekelmans and Neklyudov [2023], Vargas and Nüsken [2023], Vargas et al. [2024]. These works, however, focus on finding a path measure with distinct marginal constraints, overlooking the potential application to resampling and algorithmic simplifications obtained for the case in which the marginal constraints are the same.

Schrödinger bridges and stochastic interpolants. Schrödinger bridges have been used to obtain generative models by flowing samples from a prior distribution to an empirical data distribution from which new data is to be sampled. Several methods have been proposed to this end: De Bortoli et al. [2021], Vargas et al. [2021] iteratively estimate the drift of the SDE associated with the diffusion processes of half-bridge formulations. While the first uses neural networks and score matching, the latter employs Gaussian processes. From these, a number of extensions or alternatives have been presented; most relevant are [Shi et al., 2023, Peluchetti, 2023], which extend [De Bortoli et al., 2021] but differ with respect to the projection sets used to define their half-bridge formulations. Schrödinger-bridge-based methods alleviate the computational expense incurred by score-based generative models (SGM) [De Bortoli et al., 2021]. The latter requires the forward diffusion process to run for longer times with smaller step sizes. Unlike SGM, our method provides a tool to flow an existing sample in the same data distribution with control over the spread of the newly obtained sample.

To the best of our knowledge, the work of Albergo et al. [2023] is the only one in the literature on generative modeling that considers maps from a distribution to itself. In their paper, flow matching learns a drift function associated with a stochastic path from the data distribution to itself. Their stochastic interpolants, however, do not attempt to seek optimality in the relative entropy sense, a property correlated to sampling effectiveness and generation quality [Shaul et al., 2023]. By contrast, our method seeks to estimate the coupling with minimal relative entropy, similar in spirit to methods such as [Vargas et al., 2021, De Bortoli et al., 2021, Shi et al., 2023]; our method, however, presents certain algorithmic advantages over these, which can only be derived for the mirror case.

3 Mathematical Preliminaries

Definition. Let $n > 0$ be an integer, and let $\mathbb{P}^0 \in \mathcal{P}(C([0, 1], \mathbb{R}^n))$ be a reference measure in the space of path measures. Following [Jamison, 1975, Léonard, 2014], we define the *Schrödinger bridge problem* as the problem of finding a path measure \mathbb{P}_{SB} interpolating between prescribed initial and final marginals π_0 and π_1 that is the closest to \mathbb{P}^0 with respect to Kullback-Leibler divergence D_{KL} . To be precise, we define \mathbb{P}_{SB} to be the solution of the following optimization problem:

$$\mathbb{P}_{\text{SB}} := \arg \min_{\mathbb{P} \in \mathbb{D}(\pi_0, \pi_1)} D_{\text{KL}}(\mathbb{P} \| \mathbb{P}^0), \quad (1)$$

where $\mathbb{D}(\pi_0, \pi_1)$ denotes the set of path measures with marginals π_0 and π_1 . In other words, we say that \mathbb{P}_{SB} is the *direct D_{KL} projection* of \mathbb{P}^0 onto the space $\mathbb{D}(\pi_0, \pi_1)$.

The reference path measure \mathbb{P}^0 is typically chosen to be associated with a diffusion process, which is defined to be any stochastic process \mathbf{X}_t governed by a forward SDE

$$d\mathbf{X}_t = f_t(\mathbf{X}_t)dt + \sigma d\mathbf{W}_t,$$

where f_t is the forward drift function, $\sigma > 0$ is the noise coefficient, and \mathbf{W}_t is the Wiener process. Such a process \mathbf{X}_t corresponds to a unique path measure once an initial or final condition

is specified. An important aspect of diffusion processes is that their time-reversals are diffusion processes of the same noise coefficient σ . That is, if \mathbf{X}_t is a diffusion process with time-reversal \mathbf{Y}_t , then the ensembles $(\mathbf{Y}_t)_{t \in [0,1]}$ and $(\mathbf{X}_{1-t})_{t \in [0,1]}$ coincide, and \mathbf{Y}_t is governed by a backward SDE

$$d\mathbf{Y}_t = b_t(\mathbf{Y}_t)dt + \sigma d\mathbf{W}_t,$$

where b_t denotes the backward drift function (see [Winkler et al., 2023, §2.3]).

In the case where \mathbb{P}^0 arises from a diffusion process, any path measure with finite KL divergence with respect to \mathbb{P}^0 , including the Schrödinger bridge \mathbb{P}_{SB} , necessarily also arises from a diffusion process with noise σ [Vargas et al., 2021, Léonard, 2014]. Consequently, by adjusting the initial condition of the reference SDE, we can assume that the reference process \mathbb{P}^0 has a prescribed initial marginal π_0 , without changing the solution to (1).

Iterative Proportional Fitting Procedure. In the literature, the typical strategy for solving the problem (1) is to apply a general technique known as the *Iterative Proportional Fitting Procedure* (IPFP) [Fortet, 1940, Kullback, 1968]. This procedure obtains the Schrödinger bridge by iteratively solving the following pair of half-bridge problems:

$$\mathbb{P}^{2k+1} = \arg \min_{\mathbb{P} \in \mathbb{D}(\cdot, \pi_1)} D_{\text{KL}}(\mathbb{P} \| \mathbb{P}^{2k}), \quad \mathbb{P}^{2k+2} = \arg \min_{\mathbb{P} \in \mathbb{D}(\pi_0, \cdot)} D_{\text{KL}}(\mathbb{P} \| \mathbb{P}^{2k+1}), \quad (2)$$

where $\mathbb{D}(\cdot, \pi_1)$ (resp., $\mathbb{D}(\pi_0, \cdot)$) denotes the space of path measures with final (resp., initial) marginal π_1 (resp., π_0). Ruschendorf [1995] proves that the sequence of iterates \mathbb{P}^k converges in total variation to \mathbb{P}_{SB} as $k \rightarrow \infty$. IPFP can be thought of as an extension of Sinkhorn's algorithm to continuous state spaces, where the rescaling updates characteristic of Sinkhorn are replaced by iterated direct D_{KL} projections onto sets of distributions with fixed initial or final marginal [Essid and Pavon, 2019].

Applications. Suppose π_0 is given by a data distribution p_{data} , and take π_1 to be an easy-to-sample distribution p_{prior} , e.g., $\mathcal{N}(0, \mathbf{I})$. The backward diffusion process associated with \mathbb{P}_{SB} gives a model for sampling from p_{data} . In practice, the IPFP iterates in (2) can be solved using diffusion Schrödinger bridge (DSB), an algorithm developed by De Bortoli et al. [2021]. DSB relies on the following fact, which is a consequence of Girsanov's theorem: \mathbb{P}^{2k+1} is the path measure whose backward drift equals the time-reversal of the forward drift of \mathbb{P}^{2k} , and \mathbb{P}^{2k+2} is the path measure whose forward drift equals the time-reversal of the backward drift of \mathbb{P}^{2k+1} . Leveraging this, DSB solves for \mathbb{P}_{SB} by training neural networks to learn the forward and backward drifts associated with the IPFP iterates.

4 Mirror Schrödinger Bridges

Given a reference path measure \mathbb{P}^0 and a prescribed marginal distribution π , we consider the Schrödinger bridge problem between π and itself with respect to \mathbb{P}^0 . In the case where \mathbb{P}^0 is time-symmetric, meaning that the path measure is invariant under the transformation $t \rightarrow -t$, the Schrödinger bridge will inherit the time-symmetry

$$\mathbb{P}_{\text{MSB}} := \arg \min_{\mathbb{P} \in \mathbb{D}(\pi, \pi)} D_{\text{KL}}(\mathbb{P} \| \mathbb{P}^0), \quad (3)$$

so that $\mathbb{P}_{\text{MSB}} \in \mathbb{D}(\pi, \pi)$ is the path measure with identical prescribed marginals equal to π that is closest to the reference measure \mathbb{P}^0 with respect to the KL divergence D_{KL} .

A naïve approach to solving the mirror Schrödinger bridge problem (3) is to apply IPFP with both marginals $\pi_0 = \pi_1$ set equal to π . In practice, this requires iterative training of two neural networks f_t^θ and b_t^ϕ , the first modeling the drift of the forward diffusion process associated to \mathbb{P}_{MSB} and the latter modeling the drift of the corresponding backward process. But this straightforward application of IPFP leads to unnecessary computational expense, as it fails to use the time-symmetry of the problem (3). In particular, at optimality the forward and backward drifts of \mathbb{P}_{MSB} must be equal, because the mirror Schrödinger bridge \mathbb{P}_{MSB} is time-symmetric. Related works in entropic optimal transportation suggest that the use of one optimization variable for the static transport formulation in the symmetric case (see [Kurras, 2015, Section 3] and [Feydy et al., 2019, Equations (24)-(25)]), but to our knowledge no approach has been developed to leverage symmetry for the dynamical formulation in the language of path measures. This suggests the strategy of modeling the drift with a single neural network and using the IPFP iterations to recursively train that network. While this strategy already yields a significant simplification in the implementation of IPFP, it turns out that we can do even better by further exploiting the time-symmetry of the mirror problem.

In §4.1, we introduce a symmetrized version of IPFP, replacing the second projection with a step that enforces symmetry of the bridge iterate. In §4.2, we present the key insight that, at least to first order, this symmetrization step can be performed analytically by averaging the forward and backward drifts of the previous iterate. We show that this drift averaging can be interpreted as a minimization problem in its own right, by simply reversing the direction of the D_{KL} divergence in the symmetrization step. The resulting method is a convenient first-order approximation of symmetrized IPFP in terms of what is known in information geometry as the *Alternating Minimization Procedure* (AMP), first formalized by Csiszár and Tusnády [1984]. Then, in §4.3, we derive an efficient algorithm that trains a single neural network modeling the drift associated to \mathbb{P}_{MSB} and requires half the computational expense in terms of training iterations for the mirror problem compared to other IPFP-based algorithms.

4.1 Symmetrized Iterative Proportional Fitting

Take the reference path measure \mathbb{P}^0 to be time-symmetric. As an example, we can take \mathbb{P}^0 to be associated to an Ornstein–Uhlenbeck process \mathbf{X}_t (at equilibrium) given by an SDE of the form $d\mathbf{X}_t = -\alpha \mathbf{X}_t dt + \sigma d\mathbf{W}_t$, for $\alpha > 0$, or more generally any reversible diffusion process. We consider the following iterative scheme involving a pair of direct D_{KL} projection steps:

$$\mathbb{P}^{2k+1} = \arg \min_{\mathbb{P} \in \mathbb{D}(\pi, \cdot)} D_{KL}(\mathbb{P} \parallel \mathbb{P}^{2k}) \quad (4)$$

$$\mathbb{P}^{2k+2} = \arg \min_{\mathbb{P} \in \mathbb{S}} D_{KL}(\mathbb{P} \parallel \mathbb{P}^{2k+1}), \quad (5)$$

where \mathbb{S} is the set of time-symmetric path measures with no marginal constraints. This scheme is a dynamical analogue for path measures of the symmetrized version of Sinkhorn’s algorithm described by Kurras [2015]. Each iteration of this scheme in (4)–(5) is designed to obtain the time-symmetric measure \mathbb{P} that minimizes the objective while remaining close in D_{KL} divergence to the measure obtained in the previous half iteration, which satisfies the initial marginal constraint π . As direct D_{KL} projections satisfy the Pythagorean theorem for D_{KL} divergences, we have the following result:

Lemma 4.1. *The scheme in (4)–(5) converges to the mirror Schrödinger bridge.*

This is proven by Ruschendorf [1995]. A theoretical requirement for this scheme is that the reference measure \mathbb{P}^0 be time-symmetric, so standard Brownian motion cannot be used as a prior. As we show in §4.2, the first projection step (4) has a simple analytical solution, but the problem of computing the direct D_{KL} projection (5) onto the set \mathbb{S} of time-symmetric path measures is considerably more difficult, and it remains open as to whether this projection admits an explicit analytical description, like for the projection (4). Thus, to obtain an algorithmic improvement on IPFP that leverages the symmetry of our problem, we would like a more efficient alternative to explicitly solving (5).

4.2 Alternating Minimization Procedure (AMP)

A key insight of our paper is that the symmetrization step simplifies dramatically if we reverse the direction of the D_{KL} divergence. This motivates us to consider a modified version of our symmetrized IPFP scheme, where the D_{KL} divergence in (5) is reversed. We prove in this section that the resulting *alternating minimization scheme* (1) has a simple analytical solution for the symmetrization step, and (2) agrees with symmetrized IPFP to first order.

More precisely, take the reference path measure \mathbb{P}^0 to be time-symmetric. As an example, we can take \mathbb{P}^0 to be associated to an Ornstein–Uhlenbeck process \mathbf{X}_t given by an SDE of the form $d\mathbf{X}_t = -\alpha \mathbf{X}_t dt + \sigma d\mathbf{W}_t$, for $\alpha > 0$, or more generally any reversible diffusion process. We propose the following iterative scheme:

$$\mathbb{P}^{2k+1} = \arg \min_{\mathbb{P} \in \mathbb{D}(\pi, \cdot)} D_{KL}(\mathbb{P} \parallel \mathbb{P}^{2k}) \quad (direct) \quad (6)$$

$$\mathbb{P}^{2k+2} = \arg \min_{\mathbb{P} \in \mathbb{S}} D_{KL}(\mathbb{P}^{2k+1} \parallel \mathbb{P}), \quad (reverse) \quad (7)$$

where \mathbb{S} is the set of time-symmetric path measures with no marginal constraints. This scheme is an instance of AMP and differs from IPFP in that it alternates between direct and reverse D_{KL} projections. To see this, note that (6) is a direct D_{KL} projection and coincides with the odd-numbered steps in the IPFP iterations (2), whereas (7) is a *reverse* D_{KL} projection, as the KL divergence is being computed against the optimization parameter \mathbb{P} instead of the previously produced path measure \mathbb{P}^{2k+1} .

If for some reason \mathbb{P}^{2k+1} is not supported at a point, then the solution to the minimization in (7) may not be unique, in which case we define \mathbb{P}^{2k+2} to be any minimizer. But this is no problem: in what follows, we will prove Propositions 4.2 and 4.3, which together imply that the subsequent odd-numbered iterate \mathbb{P}^{2k+3} is always uniquely determined, regardless of the choice of \mathbb{P}^{2k+2} . We now explore each of the projections in our alternating minimization scheme in detail.

Projection (6). We can compute the direct D_{KL} projection onto the set of path measures with a prescribed initial marginal distribution π following the trajectory-caching method developed and applied by Vargas et al. [2021], De Bortoli et al. [2021]. Let π be a probability distribution on \mathbb{R}^n , and let $\mathbb{P} \in \mathbb{D}(\pi, \cdot)$ and $\mathbb{P}^\dagger \in \mathbb{S}$ be path measures corresponding to diffusion processes. Write $f_t^\mathbb{P}$ and $b_t^\mathbb{P}$ for the forward and backward drift functions corresponding to \mathbb{P} , and write $v_t^{\mathbb{P}^\dagger} = f_t^{\mathbb{P}^\dagger} = b_t^{\mathbb{P}^\dagger}$ for the drift of \mathbb{P}^\dagger . As a consequence of Girsanov's theorem, we can write $D_{\text{KL}}(\mathbb{P} \parallel \mathbb{P}^\dagger)$ explicitly in terms of $f_t^\mathbb{P}$ and $v_t^{\mathbb{P}^\dagger}$, or equivalently in terms of $b_t^\mathbb{P}$ and $v_t^{\mathbb{P}^\dagger}$; for references, see [Chen et al., 2016, §3] as well as [Winkler et al., 2023, §2.2, §2.3]. Indeed, for some constants C_1, C_2 , we have

$$D_{\text{KL}}(\mathbb{P} \parallel \mathbb{P}^\dagger) = C_1 + \frac{1}{2\sigma^2} \int_0^1 \mathbb{E}_{\mathbb{P}} \left[(f_t^\mathbb{P}(\mathbf{X}_t) - v_t^{\mathbb{P}^\dagger}(\mathbf{X}_t))^2 \right] dt \quad (8)$$

$$= C_2 + \frac{1}{2\sigma^2} \int_0^1 \mathbb{E}_{\mathbb{P}} \left[(b_t^\mathbb{P}(\mathbf{X}_t) - v_t^{\mathbb{P}^\dagger}(\mathbf{X}_t))^2 \right] dt. \quad (9)$$

In light of (8) and (9), and because drift functions are more amenable to modeling and estimation than path measures, it is convenient to recast the steps of our AMP scheme as iterative computations of drifts associated to D_{KL} projections. The following result is an immediate consequence of (8):

Proposition 4.2. *The direct D_{KL} projection of \mathbb{P}^\dagger onto the space $\mathbb{D}(\pi, \cdot)$ is given by the unique path measure \mathbb{P} with initial marginal π and forward drift $f_t^\mathbb{P}$ equal to the drift $v_t^{\mathbb{P}^\dagger}$ of \mathbb{P}^\dagger .*

In our AMP scheme, we employ Proposition 4.2 by taking $\mathbb{P} = \mathbb{P}^{2k+1} \in \mathbb{D}(\pi, \cdot)$ to have drift equal to that of $\mathbb{P}^\dagger = \mathbb{P}^{2k}$ for each $k \geq 0$.

Projection (7). As before, we are interested in computing the associated time-symmetric drift, rather than the path measure itself. To this end, let π be a probability distribution on \mathbb{R}^n , and let $\mathbb{P} \in \mathbb{D}(\pi, \cdot)$ and $\mathbb{P}^\dagger \in \mathbb{S}$ be path measures corresponding to diffusion processes. Suppose we seek to minimize $D_{\text{KL}}(\mathbb{P} \parallel \mathbb{P}^\dagger)$ over all $\mathbb{P}^\dagger \in \mathbb{S}$. Using (8) and (9), we can write $D_{\text{KL}}(\mathbb{P} \parallel \mathbb{P}^\dagger)$ explicitly in terms of the forward and backward drift functions of the SDE corresponding to the path measures \mathbb{P} and \mathbb{P}^\dagger . First, we can combine (8) and (9) to rewrite $D_{\text{KL}}(\mathbb{P} \parallel \mathbb{P}^\dagger)$ in a time-symmetric formulation as follows:

$$D_{\text{KL}}(\mathbb{P} \parallel \mathbb{P}^\dagger) = C + \frac{1}{4\sigma^2} \int_0^1 \mathbb{E}_{\mathbb{P}} \left[(f_t^\mathbb{P}(\mathbf{X}_t) - v_t^{\mathbb{P}^\dagger}(\mathbf{X}_t))^2 + (b_t^\mathbb{P}(\mathbf{X}_t) - v_t^{\mathbb{P}^\dagger}(\mathbf{X}_t))^2 \right] dt, \quad (10)$$

where C is a constant. A key benefit of considering the reverse D_{KL} projection is that the expectations in (8) and (9) are taken with respect to the fixed path measure \mathbb{P} , and not with respect to the varying \mathbb{P}^\dagger . Using calculus of variations, we can then compute a closed-form expression for the drift of the minimizer of $D_{\text{KL}}(\mathbb{P} \parallel \mathbb{P}^\dagger)$ over $\mathbb{P}^\dagger \in \mathbb{S}$. Note that the sum of squares inside the expectation on the right-hand side above is always nonnegative. Consequently, to minimize $D_{\text{KL}}(\mathbb{P} \parallel \mathbb{P}^\dagger)$, it suffices to choose $v_t^{\mathbb{P}^\dagger}$ so that it minimizes this sum of squares at each time t . Taking the first variation of this sum with respect to $v_t^{\mathbb{P}^\dagger}$, setting the result equal to zero, and solving for the optimal $v_t^{\mathbb{P}^\dagger}$, we obtain:

$$v_t^{\mathbb{P}^\dagger}(x) = \frac{1}{2} (f_t^\mathbb{P}(x) + b_t^\mathbb{P}(x)). \quad (11)$$

In other words, we have proven the following characterization of the projection (7):

Proposition 4.3. *The reverse D_{KL} projection of \mathbb{P} onto the space \mathbb{S} is a time-symmetric path measure with drift given by the average of the forward and backward drifts of \mathbb{P} .*

It is natural to ask what relation the explicit formula (11) for the minimizer of the reverse D_{KL} projection (7) has to the minimizer of the direct D_{KL} projection (5) in symmetrized IPFP. The following proposition establishes that these two minimizers agree to first order (see proof in Appendix A).

Proposition 4.4. *Let v_t^* be the drift corresponding to the minimizer of the D_{KL} projection (5). Then*

$$v_t^*(x) = \frac{1}{2} (f_t^\mathbb{P}(x) + b_t^\mathbb{P}(x)) + O(\|f_t^\mathbb{P}(x) - b_t^\mathbb{P}(x)\|^2)$$

For alternating minimization schemes, like (6)-(7), some convergence results were established by Csiszár and Tusnády [1984]. For instance, their Theorem 3 implies that the sequence whose $(2k+1)$ -th term is $D_{\text{KL}}(\mathbb{P}^{2k+1} \parallel \mathbb{P}^{2k})$ and whose $(2k+2)$ -th term is $D_{\text{KL}}(\mathbb{P}^{2k+1} \parallel \mathbb{P}^{2k+2})$ monotonically decreases to a limiting value equal to

$$D_{\text{KL}}(\mathbb{D}(\pi, \cdot), \mathbb{S}) := \inf_{\substack{\mathbb{P} \in \mathbb{D}(\pi, \cdot) \\ \mathbb{P}^\dagger \in \mathbb{S}}} D_{\text{KL}}(\mathbb{P} \parallel \mathbb{P}^\dagger).$$

But this limiting value is zero, as the intersection $\mathbb{D}(\pi, \cdot) \cap \mathbb{S}$ is nonempty. Thus, the sequence of iterates \mathbb{P}^k obtained by our AMP actually converges to a time-symmetric path measure with desired marginals (in situations where alternating projections are performed onto nonintersecting sets, convergence is much trickier to establish; e.g., for discrete probability measures, it was proven by Csiszár and Tusnády [1984] that the odd-numbered iterates converge, but the even-numbered ones may not).

The limit of our alternating scheme, while it exists, may not necessarily coincide with that of IPFP, because direct D_{KL} projections encourage mean-seeking behavior, whereas reverse D_{KL} projections encourage mode-seeking behavior. This concurs with an observation of Kurras [2015] in the static case, where they note that taking the arithmetic mean of the transport matrix and its transpose to perform the symmetrization step can cause the method to converge to a limit different from the optimal one. So far, we proved that our reversed symmetrization update agrees with the direct D_{KL} projection to first order. Thus, we expect that our alternating scheme converges to a good approximation of the Schrödinger bridge. We confirm this expectation in two different ways. First, we show that the limit of our approximate scheme is close to the Schrödinger bridge in the Gaussian case and is numerically indistinguishable from the result of IPFP; see Fig. 2 and 6. Second, we formulate reasonable hypotheses under which the difference between the mirror Schrödinger bridge and the limit of our alternating scheme, i.e., the mirror bridge, can be explicitly bounded; see Appendix B.

4.3 Practical Algorithm

We now describe an algorithm to solve the mirror bridge problem numerically, based on our AMP scheme from §4.2. We choose our reference path measure $\mathbb{P}^0 \in \mathbb{S}$ to be associated to an Ornstein-Uhlenbeck process \mathbf{X}_t given by the $d\mathbf{X}_t = -\alpha \mathbf{X}_t dt + \sigma d\mathbf{W}_t$, for $\alpha > 0$.

Recall that our AMP scheme alternates between direct D_{KL} projections on the set of path measures with initial marginal π and reverse D_{KL} projections on the set of time-symmetric path measures. We now explain how each of these projections is computed in practice. Our algorithm then follows by iteratively applying this pair of projections and is summarized in Algorithm 1.

As is evident from our analysis of the reverse D_{KL} projection, it does not suffice for us to know only the forward drift associated to our path measure iterates. We need to know the backward drift $b_t^{\mathbb{P}}$ too, but in practice, we do not have access to it. We use trajectory caching to estimate the backward drift $b_t^{\mathbb{P}}$. Trajectory caching is principled on the fact that $b_t^{\mathbb{P}}$ can be expressed in terms of the expected rate of change in \mathbf{X}_t over time. Concretely, we have the following formula, which can be taken as a formal definition of the backward drift of a diffusion process:

$$b_{1-t}^{\mathbb{P}}(x) = \lim_{\gamma \rightarrow 0} \mathbb{E} \left[\frac{\mathbf{X}_{t-\gamma} - \mathbf{X}_t}{\gamma} \mid \mathbf{X}_t = x \right]. \quad (12)$$

To apply (12) in practice, take a positive integer M and let $\{\gamma_i\}_{i=1}^M$ be a sequence of M discrete time steps with sequence of partial sums $\{\bar{\gamma}_i\}_{i=1}^M$. Then we construct a discrete representation of the stochastic process \mathbf{X}_t by using the Euler-Maruyama method to generate a collection of N sample trajectories $\{\mathbf{X}_i^j\}_{i,j=0}^{M-1,N-1}$ starting at the initial distribution π in accordance with the SDE $d\mathbf{X}_t = f_t^{\mathbb{P}}(\mathbf{X}_t)dt + \sigma d\mathbf{W}_t$, where we know the forward drift $f_t^{\mathbb{P}}$ because we matched it to the drift of \mathbb{P}^\dagger . Explicitly, we have for all $i \in \{0, \dots, M-2\}$ and $j \in \{0, \dots, N-1\}$ that

$$\mathbf{X}_{i+1}^j = \mathbf{X}_i^j + f_{\bar{\gamma}_i}^{\mathbb{P}}(\mathbf{X}_i^j)\gamma_i + \sigma^j \sqrt{\gamma_i} \mathbf{Z}_i^j, \quad (13)$$

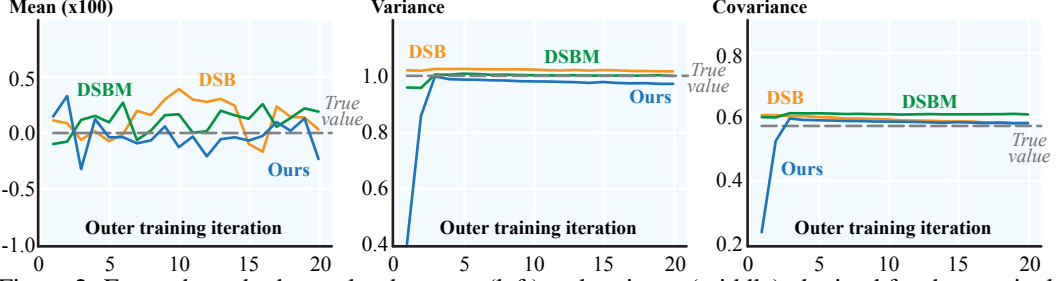


Figure 2: For each method, we plot the mean (left) and variance (middle) obtained for the terminal samples, i.e. samples obtained at time $t = T$, as well as the covariance (right) of the joint distribution, versus the number of outer iterations, averaged over 5 trials.

where $\mathbf{Z}_i^j \sim \mathcal{N}(0, \mathbf{I})$. The limiting quantity in (12) is then leveraged as the target of the loss function used to train a neural network v_t^θ , which approximates the backward drift $b_t^{\mathbb{P}}$ for a specified range of σ values $[\sigma_{\min}, \sigma_{\max}]$. Specifically, we define the loss ℓ in terms of the optimization parameter θ by

$$\ell = \frac{1}{N} \sum_{i=1}^{M-1} \sum_{j=0}^{N-1} \left\| v_{\bar{\gamma}_{i+1}}^\theta(\mathbf{X}_i^j) - \frac{\mathbf{X}_i^j - \mathbf{X}_{i+1}^j}{\bar{\gamma}_{i+1}} - \left(f_{\bar{\gamma}_i}^{\mathbb{P}^\dagger}(\mathbf{X}_{i+1}^j) - f_{\bar{\gamma}_i}^{\mathbb{P}^\dagger}(\mathbf{X}_i^j) \right) \right\|^2 \quad (14)$$

Observe that the first two terms in the loss constitute the difference between the drift and the infinitesimal rate of change of the process \mathbf{X}_t , i.e., the discretization of the difference between the left- and right-hand sides of (12). The network parameters θ are then learned via gradient descent with respect to the loss function $\ell(\theta)$. The resulting function v_t^θ , where θ minimizes the loss $\ell(\theta)$, approximates the desired backward drift, as is suggested by De Bortoli et al. [2021, Proposition 3]. In our AMP scheme, we employ (11) by averaging the forward and backward drifts corresponding to $\mathbb{P} = \mathbb{P}^{2k+1}$ to obtain the drift of the symmetric path measure $\mathbb{P}^\dagger = \mathbb{P}^{2k+2}$. Practically speaking, if the drift of \mathbb{P}^{2k} is a parametrized by a neural network $v_t^{\theta_k}$ for each k , we take the drift of \mathbb{P}^{2k+1} to be the average output of the networks $v_t^{\theta_{k-1}}$ and $v_t^{\theta_k}$. In Algorithm 1, we denote the limiting drift as $v_t^{\theta^*}$.

Sampling with in-distribution variation. We provide a short intuitive explanation of why our method allows for resampling with prescribed proximity to an input sample in Appendix C.

5 Experiments

We demonstrate the utility of our method on a number of conditional resampling tasks, illustrating how it can be used to produce sample variations with control over the proximity to the initial sample.

Gaussian transport. We start by comparing our method with two alternative algorithms, DSB [De Bortoli et al., 2021] and DSBM [Shi et al., 2023], when applied to the mirror Schrödinger bridge of multi-dimensional Gaussians. Fig. 2 shows that, in the case of dimension $d = 50$, as the number of outer iterations increases, the empirical convergence of our method performs on par with both DSB and DSBM with the added benefit that each outer iteration with our algorithm requires half the training iterations. Recall that our method trains a single neural network to model a time-symmetrized drift function v_t^θ rather than a neural network for each of the forward and backward drift functions. More details on the derivation of the analytical solution, as well as information on parameters, can be found in Appendix D. Additional results for dimensions $d = 5, 20$ can be found in Fig. 6.

2D datasets. To illustrate the behavior of our method, we use our algorithm to resample from 2-dimensional distributions Pedregosa et al. [2011]. Unlike the mirror Schrödinger bridge with Gaussians, an analytical solution with these more general distributions is not known. We consider learning the drift function v_t^θ associated with the mirror bridge that flows samples from p_{data} to itself.

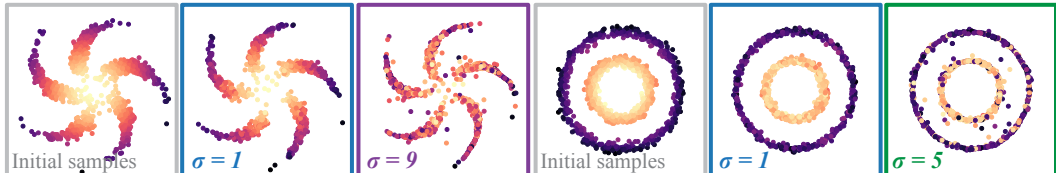


Figure 3: Samples (color based on initial position) obtained using our method with various σ values.

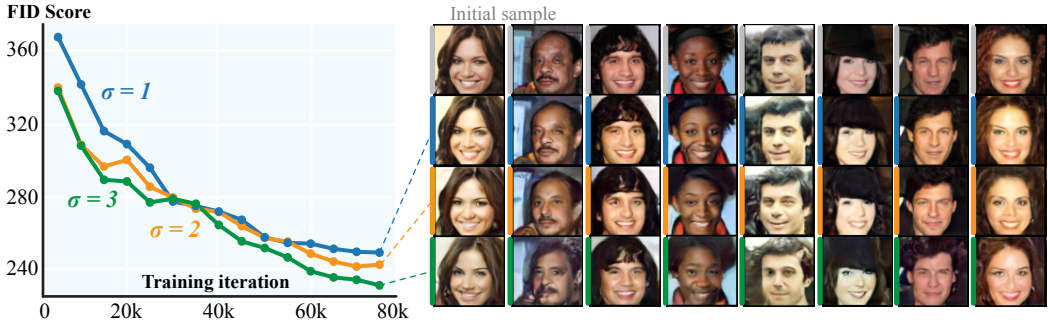


Figure 5: The control over in-distribution variance effect of σ for a variety of initial samples (first row) from the empirical distribution of images in the CelebA dataset.

The goal is to obtain new samples that are in the distribution p_{data} but exhibit some level of variation, i.e., in-distribution variation, correlated to the noise coefficient σ in the diffusion process.

In Fig. 3, we show the result of flowing samples via the mirror bridge with varying values of noise. We observe that the in-distribution variation of data points is controlled by the choice of σ value, which can indeed be detected by the mixing of colors, or lack of thereof, in each terminal distribution shown. For instance, on the right, we find mixing from samples between the inner and outer circles with the largest σ value, compared with no mixing between circles with the smallest σ value.

Image resampling. We train our algorithm on the MNIST LeCun et al. [1998] and CelebA Liu et al. [2015] datasets. Training parameters and architecture for all experiments can be found in Appendix E. Our results show that mirror bridges can be used to produce new samples from an image dataset with control over the proximity to the initial sample. In Fig. 4, we resample from MNIST using varying levels of noise (see also Fig. 11). Pushforward images obtained with a lower σ value (*middle*) are visually closer to the initial images (*top*) than the ones obtained with a higher σ value (*bottom*).



Figure 4: Samples produced by our mirror bridges for MNIST, using $\sigma = 1, 2$.

Fig. 5 shows the same control over in-distribution variation of pushforward samples using the RGB dataset CelebA. In each column, we exhibit a different sample from the dataset and, in each row, we show the corresponding push-forward obtained for different noise values. These results can be obtained without retraining the neural network. The typical metric to assess resampling quality for the image generation case is the Fréchet inception distance (FID) score, which we have plotted against training iterations.

We observe FID scores decreasing with training iterations.

Fig. 12 includes more results using the CelebA dataset, and Fig. 7 shows the nearest neighbors in the dataset to the generated images. In the latter, the nearest neighbor of the generated sample is the initial sample itself, and the generated sample is distinct from all of its nearest neighbors, showing that our model does not simply regurgitate nearest neighbors of the initial sample as proximal outputs. Additional experiments, including a comparison to alternative methods for image resampling, further evaluation metrics, results on path regularity and control over proximity, are presented in Appendix F.

6 Conclusion

By studying an overlooked version of the Schrödinger bridge problem, which we coin the *mirror bridge*, we present an algorithm to sample with control over the in-distribution variation of new data points. Our method is flexible and requires fewer training iterations than existing alternatives [De Bortoli et al., 2021, Shi et al., 2023] designed for the general Schrödinger bridge problem. As a technique for estimating Schrödinger bridges in the mirror case, our method presents an advantage over mirror interpolants [Albergo et al., 2023], since optimizing the relative entropy of such an interpolant results in a min-max optimization problem that is typically intractable [Shaul et al., 2023]. Our method is numerically tractable and well-principled, and it cuts down training in applications where control over in-distribution variation is desired. On the application front, we demonstrate that our method is a flexible tool to obtain new data points from empirical distributions in a variety of domains, including 2-dimensional measures and image datasets. In future work, we hope to study of a potential σ threshold for a sample to change class when resampled or to make “class” a neural network input, similar to text prompting in image generation.

Acknowledgments and Disclosure of Funding

The authors would like to thank Lingxiao Li, Artem Lukoianov and Christopher Scarvelis for discussion and feedback. We are also grateful to Suvrit Sra for thoughtful insights on related work. We thank Ahmed Mahmoud for proofreading. Leticia Mattos Da Silva acknowledges the generous support of a MathWorks Engineering Fellowship. The MIT Geometric Data Processing Group acknowledges the generous support of Army Research Office grants W911NF2010168 and W911NF2110293, of National Science Foundation grant IIS2335492, from the CSAIL Future of Data program, from the MIT–IBM Watson AI Laboratory, from the Wistron Corporation, and from the Toyota–CSAIL Joint Research Center.

References

- Medha Agarwal, Zaid Harchaoui, Garrett Mulcahy, and Soumik Pal. Iterated Schrödinger bridge approximation to Wasserstein gradient flows, 2024. URL <https://arxiv.org/abs/2406.10823>.
- Michael S. Albergo, Nicholas M. Boffi, and Eric Vanden-Eijnden. Stochastic interpolants: A unifying framework for flows and diffusions, 2023. URL <https://arxiv.org/abs/2303.08797>.
- Rob Brekelsmans and Kirill Neklyudov. On Schrödinger bridge matching and expectation maximization. In *NeurIPS 2023 Workshop Optimal Transport and Machine Learning*, 2023. URL <https://openreview.net/forum?id=Bd4DTPzOGO>.
- Yongxin Chen, Tryphon T. Georgiou, and Michele Pavon. On the relation between optimal transport and Schrödinger bridges: a stochastic control viewpoint. *J. Optim. Theory Appl.*, 169(2):671–691, 2016. ISSN 0022-3239,1573-2878. doi: 10.1007/s10957-015-0803-z. URL <https://doi.org/10.1007/s10957-015-0803-z>.
- Nicolas Courty, Rémi Flamary, Devis Tuia, and Alain Rakotomamonjy. Optimal transport for domain adaptation. *IEEE Trans. Pattern Anal. Mach. Intell.*, 39(9):1853–1865, sep 2017. ISSN 0162-8828.
- Imre Csiszár and Gábor Tusnády. Information geometry and alternating minimization procedures. pages 205–237. 1984. Recent results in estimation theory and related topics.
- Marco Cuturi. Sinkhorn distances: Lightspeed computation of optimal transport. In C.J. Burges, L. Bottou, M. Welling, Z. Ghahramani, and K.Q. Weinberger, editors, *Advances in Neural Information Processing Systems*, volume 26. Curran Associates, Inc., 2013. URL https://proceedings.neurips.cc/paper_files/paper/2013/file/af21d0c97db2e27e13572cbf59eb343d-Paper.pdf.
- Valentin De Bortoli, James Thornton, Jeremy Heng, and Arnaud Doucet. Diffusion Schrödinger bridge with applications to score-based generative modeling. In A. Beygelzimer, Y. Dauphin, P. Liang, and J. Wortman Vaughan, editors, *Advances in Neural Information Processing Systems*, 2021. URL <https://openreview.net/forum?id=9BnCwiXB0t>.
- W. Edwards Deming and Frederick F. Stephan. On a Least Squares Adjustment of a Sampled Frequency Table When the Expected Marginal Totals are Known. *The Annals of Mathematical Statistics*, 11(4):427 – 444, 1940. doi: 10.1214/aoms/1177731829. URL <https://doi.org/10.1214/aoms/1177731829>.
- Montacer Essid and Michele Pavon. Traversing the Schrödinger bridge strait: Robert Fortet’s marvelous proof redux. *J. Optim. Theory Appl.*, 181(1):23–60, 2019. ISSN 0022-3239,1573-2878. doi: 10.1007/s10957-018-1436-9. URL <https://doi.org/10.1007/s10957-018-1436-9>.
- Jean Feydy, Thibault Séjourné, François-Xavier Vialard, Shun-ichi Amari, Alain Trouvé, and Gabriel Peyré. Interpolating between optimal transport and mmd using sinkhorn divergences. In *The 22nd International Conference on Artificial Intelligence and Statistics*, pages 2681–2690. PMLR, 2019.
- Robert Fortet. Résolution d’un système d’équations de M. Schrödinger. *J. Math. Pures Appl. (9)*, 19: 83–105, 1940. ISSN 0021-7824.

Kaiming He, Xiangyu Zhang, Shaoqing Ren, and Jian Sun. Deep residual learning for image recognition. In *Proceedings of the IEEE conference on computer vision and pattern recognition*, pages 770–778, 2016.

Jonathan Ho, Ajay Jain, and Pieter Abbeel. Denoising diffusion probabilistic models. In H. Larochelle, M. Ranzato, R. Hadsell, M.F. Balcan, and H. Lin, editors, *Advances in Neural Information Processing Systems*, volume 33, pages 6840–6851. Curran Associates, Inc., 2020. URL https://proceedings.neurips.cc/paper_files/paper/2020/file/4c5bcfec8584af0d967f1ab10179ca4b-Paper.pdf.

Benton Jamison. The Markov processes of Schrödinger. *Z. Wahrscheinlichkeitstheorie und Verw. Gebiete*, 32(4):323–331, 1975. doi: 10.1007/BF00535844. URL <https://doi.org/10.1007/BF00535844>.

Harold W. Kuhn. The Hungarian method for the assignment problem. *Naval Research Logistics Quarterly*, 2(1-2):83–97, 1955.

Solomon Kullback. Probability Densities with Given Marginals. *The Annals of Mathematical Statistics*, 39(4):1236 – 1243, 1968.

Sven Kurras. Symmetric Iterative Proportional Fitting. In Guy Lebanon and S. V. N. Vishwanathan, editors, *Proceedings of the Eighteenth International Conference on Artificial Intelligence and Statistics*, volume 38 of *Proceedings of Machine Learning Research*, pages 526–534, San Diego, California, USA, 09–12 May 2015. PMLR.

Yann LeCun, Corinna Cortes, and CJ Burges. The mnist database of handwritten digits. <http://yann.lecun.com/exdb/mnist/>, 1998.

Christian Léonard. *Some Properties of Path Measures*, pages 207–230. Springer International Publishing, Cham, 2014. ISBN 978-3-319-11970-0. doi: 10.1007/978-3-319-11970-0_8. URL https://doi.org/10.1007/978-3-319-11970-0_8.

Christian Léonard. A survey of the Schrödinger problem and some of its connections with optimal transport. *Discrete Contin. Dyn. Syst.*, 34(4):1533–1574, 2014. ISSN 1078-0947,1553-5231. doi: 10.3934/dcds.2014.34.1533. URL <https://doi.org/10.3934/dcds.2014.34.1533>.

Ziwei Liu, Ping Luo, Xiaogang Wang, and Xiaoou Tang. Deep learning face attributes in the wild. In *Proceedings of International Conference on Computer Vision (ICCV)*, December 2015.

Arthur Mensch, Mathieu Blondel, and Gabriel Peyré. Geometric losses for distributional learning. In *International Conference on Machine Learning*, pages 4516–4525. PMLR, 2019.

Nikolas Nüsken and Lorenz Richter. Solving high-dimensional Hamilton-Jacobi-Bellman PDEs using neural networks: perspectives from the theory of controlled diffusions and measures on path space. *Partial Differ. Equ. Appl.*, 2(4):Paper No. 48, 48, 2021. ISSN 2662-2963,2662-2971. doi: 10.1007/s42985-021-00102-x. URL <https://doi.org/10.1007/s42985-021-00102-x>.

F. Pedregosa, G. Varoquaux, A. Gramfort, V. Michel, B. Thirion, O. Grisel, M. Blondel, P. Prettenhofer, R. Weiss, V. Dubourg, J. Vanderplas, A. Passos, D. Cournapeau, M. Brucher, M. Perrot, and E. Duchesnay. Scikit-learn: Machine learning in Python. *Journal of Machine Learning Research*, 12:2825–2830, 2011.

Stefano Peluchetti. Diffusion bridge mixture transports, Schrödinger bridge problems and generative modeling. *Journal of Machine Learning Research*, 24(374):1–51, 2023. URL <http://jmlr.org/papers/v24/23-0527.html>.

Ludger Ruschendorf. Convergence of the Iterative Proportional Fitting Procedure. *The Annals of Statistics*, 23(4):1160 – 1174, 1995.

Michael E. Sander, Pierre Ablin, Mathieu Blondel, and Gabriel Peyré. Sinkformers: Transformers with doubly stochastic attention. In Gustau Camps-Valls, Francisco J. R. Ruiz, and Isabel Valera, editors, *International Conference on Artificial Intelligence and Statistics, AISTATS 2022, 28-30 March 2022, Virtual Event*, volume 151 of *Proceedings of Machine Learning Research*, pages 3515–3530. PMLR, 2022. URL <https://proceedings.mlr.press/v151/sander22a.html>.

- Erwin Schrödinger. Sur la théorie relativiste de l'électron et l'interprétation de la mécanique quantique. *Annales de l'institut Henri Poincaré*, 3:269–310, 1932. URL http://dml.mathdoc.fr/item/AIHP_1932__2_4_269_0.
- Neta Shaul, Ricky T. Q. Chen, Maximilian Nickel, Matt Le, and Yaron Lipman. On kinetic optimal probability paths for generative models. In *Proceedings of the 40th International Conference on Machine Learning*, ICML’23. JMLR.org, 2023.
- Yuyang Shi, Valentin De Bortoli, George Deligiannidis, and Arnaud Doucet. Conditional simulation using diffusion Schrödinger bridges. In James Cussens and Kun Zhang, editors, *Proceedings of the Thirty-Eighth Conference on Uncertainty in Artificial Intelligence*, volume 180 of *Proceedings of Machine Learning Research*, pages 1792–1802. PMLR, 01–05 Aug 2022. URL <https://proceedings.mlr.press/v180/shi22a.html>.
- Yuyang Shi, Valentin De Bortoli, Andrew Campbell, and Arnaud Doucet. Diffusion Schrödinger bridge matching. In *Thirty-seventh Conference on Neural Information Processing Systems*, 2023. URL <https://openreview.net/forum?id=qy070HsJT5>.
- Richard Sinkhorn. A relationship between arbitrary positive matrices and doubly stochastic matrices. *Annals of Mathematical Statistics*, 35:876–879, 1964.
- Yang Song and Stefano Ermon. Generative modeling by estimating gradients of the data distribution. In H. Wallach, H. Larochelle, A. Beygelzimer, F. d’Alché-Buc, E. Fox, and R. Garnett, editors, *Advances in Neural Information Processing Systems*, volume 32. Curran Associates, Inc., 2019. URL https://proceedings.neurips.cc/paper_files/paper/2019/file/3001ef257407d5a371a96dc947c7d93-Paper.pdf.
- Yang Song and Stefano Ermon. Improved techniques for training score-based generative models. In *Proceedings of the 34th International Conference on Neural Information Processing Systems*, NIPS ’20, Red Hook, NY, USA, 2020. Curran Associates Inc. ISBN 9781713829546.
- Yang Song, Jascha Sohl-Dickstein, Diederik P Kingma, Abhishek Kumar, Stefano Ermon, and Ben Poole. Score-based generative modeling through stochastic differential equations. In *International Conference on Learning Representations*, 2021. URL <https://openreview.net/forum?id=PxTIG12RRHS>.
- Pece Trajanovski, Petar Jolakoski, Kiril Zelenkovski, Alexander Iomin, Ljupco Kocarev, and Trifce Sandev. Ornstein-Uhlenbeck process and generalizations: particle dynamics under comb constraints and stochastic resetting. *Phys. Rev. E*, 107(5):Paper No. 054129, 18, 2023. ISSN 2470-0045,2470-0053. doi: 10.1103/physreve.107.054129. URL <https://doi.org/10.1103/physreve.107.054129>.
- Francisco Vargas and Nikolas Nüsken. Transport, VI, and diffusions. In *ICML Workshop on New Frontiers in Learning, Control, and Dynamical Systems*, 2023. URL <https://openreview.net/forum?id=Ay1b1W7Mjy>.
- Francisco Vargas, Pierre Thodoroff, Austen Lamacraft, and Neil Lawrence. Solving Schrödinger bridges via maximum likelihood. *Entropy*, 23(9), 2021.
- Francisco Vargas, Shreyas Padhy, Denis Blessing, and Nikolas Nüsken. Transport meets variational inference: Controlled monte carlo diffusions. In *The Twelfth International Conference on Learning Representations*, 2024. URL <https://openreview.net/forum?id=PP1rudnxiW>.
- Ashish Vaswani, Noam Shazeer, Niki Parmar, Jakob Uszkoreit, Llion Jones, Aidan N Gomez, Łukasz Kaiser, and Illia Polosukhin. Attention is all you need. In I. Guyon, U. Von Luxburg, S. Bengio, H. Wallach, R. Fergus, S. Vishwanathan, and R. Garnett, editors, *Advances in Neural Information Processing Systems*, volume 30. Curran Associates, Inc., 2017.
- Ludwig Winkler, Cesar Ojeda, and Manfred Opper. A score-based approach for training schrödinger bridges for data modelling. *Entropy*, 25(2), 2023. ISSN 1099-4300. doi: 10.3390/e25020316. URL <https://www.mdpi.com/1099-4300/25/2/316>.
- Linqi Zhou, Aaron Lou, Samar Khanna, and Stefano Ermon. Denoising diffusion bridge models. In *The Twelfth International Conference on Learning Representations*, 2024. URL <https://openreview.net/forum?id=FKksTayvGo>.

A Proof of Proposition 4.4

As before, we are interested in computing the associated time-symmetric drift, rather than the path measure itself. To this end, let π be a probability distribution on \mathbb{R}^n , and let $\mathbb{P} \in \mathbb{S}$ and $\mathbb{P}^\dagger \in \mathbb{D}(\pi, \cdot)$ be path measures corresponding to diffusion processes. Suppose we seek to minimize $D_{\text{KL}}(\mathbb{P} \parallel \mathbb{P}^\dagger)$ over all $\mathbb{P} \in \mathbb{S}$. Let $a_t^\pm = \frac{1}{2}(f_t^{\mathbb{P}^\dagger} \pm b_t^{\mathbb{P}^\dagger})$, and recall from (10) that we have the following expression:

$$\begin{aligned} D_{\text{KL}}(\mathbb{P} \parallel \mathbb{P}^\dagger) &= C + \frac{1}{4\sigma^2} \int_0^1 \mathbb{E}_{\mathbb{P}} \left[(v_t^{\mathbb{P}}(\mathbf{X}_t) - f_t^{\mathbb{P}^\dagger}(\mathbf{X}_t))^2 + (v_t^{\mathbb{P}}(\mathbf{X}_t) - b_t^{\mathbb{P}^\dagger}(\mathbf{X}_t))^2 \right] dt \\ &= C + \frac{1}{2\sigma^2} \int_0^1 \mathbb{E}_{\mathbb{P}} \left[(v_t^{\mathbb{P}}(\mathbf{X}_t) - a_t^+(\mathbf{X}_t))^2 + a_t^-(\mathbf{X}_t)^2 \right] dt, \end{aligned}$$

where C is a constant. We now apply calculus of variations to compute the desired series expansion for the drift of the minimizer of $D_{\text{KL}}(\mathbb{P} \parallel \mathbb{P}^\dagger)$ over $\mathbb{P} \in \mathbb{S}$. To take the first variation of this D_{KL} divergence with respect to $v_t^{\mathbb{P}}$, we apply the product rule, first differentiating the argument of the expectation, and then differentiating the expectation operator itself. The calculation of the first variation of this sort of D_{KL} divergence has been performed before in the literature; see, e.g., [Nüsken and Richter, 2021, section A.2, proof of Proposition 4.3] for the full details. We reproduce the calculation here for the sake of completeness.

Let $\epsilon > 0$, and let h be a test function. Let \mathbb{P}_ϵ denote the path measure corresponding to the perturbed drift function $v_t^{\mathbb{P}_\epsilon} := v_t^{\mathbb{P}} + \epsilon h$. Then using the Radon-Nikodym derivative $d\mathbb{P}_\epsilon/d\mathbb{P}$ to rewrite the expectation in \mathbb{P}_ϵ in terms of an expectation in \mathbb{P} , we find that

$$\begin{aligned} \frac{\partial}{\partial \epsilon} \mathbb{E}_{\mathbb{P}_\epsilon} \left[\int_0^1 (v_t^{\mathbb{P}_\epsilon}(\mathbf{X}_t) - a_t^+(\mathbf{X}_t))^2 + a_t^-(\mathbf{X}_t)^2 dt \right] \Big|_{\epsilon=0} &= \\ \frac{\partial}{\partial \epsilon} \mathbb{E}_{\mathbb{P}} \left[\frac{d\mathbb{P}_\epsilon}{d\mathbb{P}} \int_0^1 (v_t^{\mathbb{P}_\epsilon}(\mathbf{X}_t) - a_t^+(\mathbf{X}_t))^2 + a_t^-(\mathbf{X}_t)^2 dt \right] \Big|_{\epsilon=0} &= \\ \mathbb{E}_{\mathbb{P}} \left[\frac{d\mathbb{P}_\epsilon}{d\mathbb{P}} \Big|_{\epsilon=0} \left(\int_0^1 2h(\mathbf{X}_t) \cdot (v_t^{\mathbb{P}}(\mathbf{X}_t) - a_t^+(\mathbf{X}_t)) dt \right. \right. & \\ \left. \left. + \int_0^1 ((v_t^{\mathbb{P}}(\mathbf{X}_t) - a_t^+(\mathbf{X}_t))^2 + a_t^-(\mathbf{X}_t)^2) dt \cdot \left(\frac{\partial}{\partial \epsilon} \log \frac{d\mathbb{P}_\epsilon}{d\mathbb{P}} \right) \Big|_{\epsilon=0} \right) \right]. \end{aligned} \tag{15}$$

where the second step above follows from the Radon-Nikodym Theorem, and where the third step above follows from the product rule and the definition of the logarithmic derivative.

To simplify the right-hand side of (15), we first note that $(d\mathbb{P}_\epsilon/d\mathbb{P})|_{\epsilon=0} = 1$. Secondly, we can apply Girsanov's Theorem to obtain a formula for $d\mathbb{P}_\epsilon/d\mathbb{P}$ as follows:

$$\frac{d\mathbb{P}_\epsilon}{d\mathbb{P}} = \exp \left(-\epsilon \int_0^1 h(\mathbf{X}_t) dW_t - \frac{\epsilon^2}{2} \int_0^1 |h(\mathbf{X}_t)|^2 dW_t \right). \tag{16}$$

Differentiating the logarithm of (16) with respect to ϵ and setting $\epsilon = 0$ then yields

$$\left(\frac{\partial}{\partial \epsilon} \log \frac{d\mathbb{P}_\epsilon}{d\mathbb{P}} \right) \Big|_{\epsilon=0} = - \int_0^1 h(\mathbf{X}_t) dW_t. \tag{17}$$

Let T denote the linear map defined on test functions by $h \mapsto - \int_0^1 h(\mathbf{X}_t) dW_t$. Then combining the right-hand side of (15) with (17), we obtain the following expression:

$$\int_0^1 \mathbb{E}_{\mathbb{P}} \left[2h \cdot (v_t^{\mathbb{P}}(\mathbf{X}_t) - a_t^+(\mathbf{X}_t)) + \left((v_t^{\mathbb{P}}(\mathbf{X}_t) - a_t^+(\mathbf{X}_t))^2 + a_t^-(\mathbf{X}_t)^2 \right) \cdot T(h) \right] dt. \tag{18}$$

For the quantity in (18) to be zero for every possible choice of the test function h , we must have that the linear map

$$h \mapsto 2h \cdot (v_t^{\mathbb{P}}(\mathbf{X}_t) - a_t^+(\mathbf{X}_t)) + \left((v_t^{\mathbb{P}}(\mathbf{X}_t) - a_t^+(\mathbf{X}_t))^2 + a_t^-(\mathbf{X}_t)^2 \right) \cdot T(h) \tag{19}$$

is identically zero. Setting this map equal to zero and solving for $v_t^{\mathbb{P}}$ yields the desired first-order approximation $v_t^{\mathbb{P}} = a_t^+ + O(\|a_t^-\|^2)$. \square

B Heuristic Bound on Our Estimation

To understand whether our AMP yields a viable estimate of the MSB, it would be useful to be able to quantify the difference between the limit of our AMP and the MSB. In this section, we provide conditions on the marginal distribution π and on the reference path measure \mathbb{P}^0 under which we can explicitly bound the difference. The conditions we include here are modeled after the work of Vargas et al. [2021], who also develop schemes for approximating Schrödinger bridges; see, e.g., Conjecture 1 in their Appendix F.

To do this, we first introduce the following terminology: given a path measure \mathbb{P} , define the following three projections:

$$\begin{aligned}\Pi(\mathbb{P}) &= \arg \min_{\mathbb{Q} \in \mathbb{D}(\pi, \cdot)} D_{\text{KL}}(\mathbb{Q} \parallel \mathbb{P}) && \text{(direct)} \\ \Phi(\mathbb{P}) &= \arg \min_{\mathbb{Q} \in \mathbb{S}} D_{\text{KL}}(\mathbb{Q} \parallel \mathbb{P}) && \text{(direct)} \\ \Psi(\mathbb{P}) &= \arg \min_{\mathbb{Q} \in \mathbb{S}} D_{\text{KL}}(\mathbb{P} \parallel \mathbb{Q}), && \text{(reverse)}\end{aligned}$$

Let $\|\cdot\|_{\text{TV}}$ denote the total variation metric on path measures. We then have the following result.

Proposition B.1. *Let the iterates of our AMP be denoted by \mathbb{P}^k , and let the iterates of symmetrized IPFP be denoted by \mathbb{Q}^k . Choose a compact ball \mathcal{C} in the total variation metric containing all of the iterates \mathbb{P}^k and \mathbb{Q}^k . Suppose the following conditions hold:*

- On \mathcal{C} , the projection (4) is a contraction, meaning that it is Lipschitz continuous with respect to the total variation metric as a function of the second argument with Lipschitz constant $L < 1$. I.e., $\|\Pi(\mathbb{P}_1) - \Pi(\mathbb{P}_2)\|_{\text{TV}} \leq L \cdot \|\mathbb{P}_1 - \mathbb{P}_2\|_{\text{TV}}$ for every choice of path measures $\mathbb{P}_1, \mathbb{P}_2 \in \mathcal{C}$.
- On \mathcal{C} , the projection (5) is non-expansive, meaning that it is Lipschitz continuous with respect to the total variation metric as a function of the second argument with Lipschitz constant $L' \leq 1$. I.e., $\|\Phi(\mathbb{P}_1) - \Phi(\mathbb{P}_2)\|_{\text{TV}} \leq L' \cdot \|\mathbb{P}_1 - \mathbb{P}_2\|_{\text{TV}}$ for every choice of path measures $\mathbb{P}_1, \mathbb{P}_2 \in \mathcal{C}$.
- For some $\varepsilon > 0$, we have $\|\Phi(\Pi(\mathbb{P})) - \Psi(\Pi(\mathbb{P}))\|_{\text{TV}} < \varepsilon$ for every choice of $\mathbb{P} \in \mathcal{C}$.

Then the total variation between the MSB and the limit of our AMP is bounded above by $\varepsilon/(1 - L)$.

Proof. We claim that the three conditions imply the following inequality:

$$\|\mathbb{P}^{2k+3} - \mathbb{Q}^{2k+3}\|_{\text{TV}} \leq L(\varepsilon + \|\mathbb{P}^{2k+1} - \mathbb{Q}^{2k+1}\|_{\text{TV}}). \quad (20)$$

To see why the claim holds, notice that the first condition implies

$$\|\mathbb{P}^{2k+3} - \mathbb{Q}^{2k+3}\|_{\text{TV}} \leq L(\|\mathbb{P}^{2k+2} - \mathbb{Q}^{2k+2}\|_{\text{TV}}). \quad (21)$$

Next, by an application of the triangle inequality followed by an application of the second and third conditions, we have

$$\begin{aligned}\|\mathbb{P}^{2k+2} - \mathbb{Q}^{2k+2}\|_{\text{TV}} &\leq \|\Psi(\mathbb{P}^{2k+1}) - \Phi(\mathbb{Q}^{2k+1})\|_{\text{TV}} \\ &\leq \|\Psi(\mathbb{P}^{2k+1}) - \Phi(\mathbb{P}^{2k+1})\|_{\text{TV}} + \|\Phi(\mathbb{P}^{2k+1}) - \Phi(\mathbb{Q}^{2k+1})\|_{\text{TV}} \\ &\leq \varepsilon + L' \cdot \|\mathbb{P}^{2k+1} - \mathbb{Q}^{2k+1}\|_{\text{TV}}.\end{aligned} \quad (22)$$

Combining the bounds (21) and (22) with the assumption that $L' \leq 1$ yields (20). Solving this recursive inequality and letting $k \rightarrow \infty$ then yields the bound in the proposition. \square

We now explain the conditions stipulated in Proposition B.1 in words. The existence of the compact ball \mathcal{C} is guaranteed because both sequences of iterates converge. The first two conditions, that the projection (4) is a contraction and that the projection (5) is non-expansive, are to be expected because metric projection maps onto convex sets are non-expansive (i.e., are Lipschitz with constant ≤ 1); note that this heuristic is not a proof of the condition, because the direct projection is computed using

the D_{KL} divergence, which is not a metric. The Lipschitz constant L depends only on the choice of the marginal π , which in our practical implementation corresponds to the data distribution.

As for the third condition, this roughly corresponds to stipulating that the reference process is not too far from the MSB, so that the reverse and direct D_{KL} projections of odd-numbered iterates are not too different from each other. Depending on how close L is to 1, the parameter ε can be made to be sufficiently small by choosing the reference process accordingly so as to ensure that the limit of the AMP is within a prescribed distance from the MSB. If one does not have the freedom to choose the reference process but would still like to obtain an estimate of the MSB quickly, one can apply a few iterations of symmetrized IPFP to obtain an intermediary time-symmetric process $\tilde{\mathbb{P}}$ that is close enough to the MSB; this intermediary process can then be used as a reference for an application of our AMP. If $\tilde{\mathbb{P}}$ is sufficiently close to the MSB, then the third condition will be satisfied on the AMP iterates for a given $\varepsilon > 0$. This mixed algorithm enjoys the speed improvement provided by our AMP, while retaining a prescribed level of accuracy.

C Sampling with In-Distribution Variation

Given such a sample $x_0 \sim \pi$, we solve the SDE corresponding to the Schrödinger bridge to push x_0 forward in time, arriving at a final sample $x_1 \in \pi$. We want x_1 to be a variation of x_0 , where the proximity of x_1 to x_0 correlates with the size of the noise coefficient σ . Justifying this mathematically requires understanding how the conditional distribution $\mathbf{X}_1 \mid \mathbf{X}_0 = x_0$, specifically its mean and variance, depend on σ . While these quantities do not in general have closed form expressions, it is possible to compute them exactly in the case where $\pi = \mathcal{N}(0, \mathbf{I})$ is a 1-dimensional Gaussian.

In this case, let \mathbf{X}_t be the diffusion process associated to the Schrödinger bridge, where the reference path measure corresponds to an Ornstein-Uhlenbeck process with drift coefficient $-\alpha$. In Proposition D.1 (see Appendix D for the statement and proof) we determine the joint distribution of \mathbf{X}_0 and \mathbf{X}_1 in terms of a quantity β , which is a function of α and σ that grows approximately as $1 + c(\alpha) \times \sigma^2$ for some function c . Let $p(x, y)$ denote the probability density function of the joint distribution of \mathbf{X}_0 and \mathbf{X}_1 , and recall that $p(x, y)$ is the product of the conditional PDF of $\mathbf{X}_1 \mid \mathbf{X}_0$ with the PDF of \mathbf{X}_0 . Using this fact in conjunction with Proposition D.1, the PDF of $\mathbf{X}_1 \mid \mathbf{X}_0 = x_0$ is

$$\frac{p(x_0, y)}{p_{\mathbf{X}_0}(x_0)} = \exp\left(-\frac{1}{2(1 - \beta^2)}(x_0^2 - 2\beta x_0 y + y^2) + \frac{x_0^2}{2}\right).$$

From the right-hand side, we see that $\mathbf{X}_1 \mid \mathbf{X}_0 = x_0$ is Gaussian with mean $x_0(\beta/1 - \beta^2)$ and variance $1 - \beta^2$. Thus, changing the noise value σ alters both the mean and variance of samples pushed forward via the Schrödinger bridge. Indeed, in the case of the mean, it grows inversely proportional to σ^2 . Consequently, if $\sigma < 1$, then we should expect the Schrödinger bridge to push samples away from the distribution mean, whereas if $\sigma > 1$, then the opposite occurs, and samples experience mean reversion. As for the variance, note that $1 - \beta^2$ grows at least as fast as σ^2 , so we should expect the Schrödinger bridge to produce samples with spread that increases as σ increases. We expect that similar effects occur even when the marginal distribution π is not Gaussian: i.e., the value of σ should be directly related to the proximity of generated samples in an analogous way. As our method gives an approximation of the true mirror Schrödinger bridge, we expect the mirror bridge to inherit these properties.

D Analytical Solution to MSB in the Gaussian Case

Proposition D.1. *Consider the static Schrödinger bridge problem with initial and final marginals equal to the d -dimensional Gaussian distribution with zero mean and unit variance, where we take the reference measure π^0 corresponding to the OU process $d\mathbf{X}_t = -\alpha\mathbf{X}_t dt + \sigma d\mathbf{W}_t$ running from $t = 0$ to $t = 1$. The solution π^* to this problem is a $2d$ -dimensional Gaussian with zero mean and covariance matrix Σ given by*

$$\Sigma = \begin{pmatrix} \Sigma_{00} & \Sigma_{01} \\ \Sigma_{10} & \Sigma_{11} \end{pmatrix} = \begin{pmatrix} \mathbf{I} & \beta\mathbf{I} \\ \beta\mathbf{I} & \mathbf{I} \end{pmatrix}, \quad \text{where } \beta = \frac{\sigma^2(1 - e^{2\alpha}) + \sqrt{16e^{2\alpha}\alpha^2 + \sigma^4(1 - e^{2\alpha})^2}}{4\alpha e^\alpha}$$

Proof. We follow the proof of Proposition 46 of De Bortoli et al. [2021], which established the corresponding result in the case where the reference process has zero drift. Imitating the proof of

Proposition 43 of De Bortoli et al. [2021], we see that the static Schrödinger bridge π^* exists and is a $2d$ -dimensional Gaussian. That the mean equals zero follows from the fact that both marginals have zero mean. The rest of the proof is devoted to determining the covariance matrix Σ of π^* .

The fact that marginals have unit variance implies that $\Sigma_{00} = \Sigma_{11} = \mathbf{I}$. To compute Σ_{01} and Σ_{10} , we start by computing the probability density function (PDF) $p^0(x, y)$ of the reference measure π^0 , where $x, y \in \mathbb{R}^d$. Recall that $p^0(x, y)$ is the product of the conditional PDF of $\mathbf{X}_1 | \mathbf{X}_0$ with the PDF of \mathbf{X}_0 . Thus, we have

$$p^0(x, y) = p_{\mathbf{X}_1 | \mathbf{X}_0}(x, y) \times p_{\mathbf{X}_0}(x).$$

Note that \mathbf{X}_0 has zero mean and unit variance, so up to normalization we have

$$p_{\mathbf{X}_0}(x) \propto e^{-\frac{x^2}{2}}.$$

On the other hand, the mean and variance of the conditional distribution $\mathbf{X}_1 | \mathbf{X}_0$ are computed in section II of Trajanovski et al. [2023], where it is shown that they are respectively given by

$$xe^{-\alpha} \quad \text{and} \quad \sigma_1^2 := \frac{\sigma^2}{2\alpha}(1 - e^{-2\alpha}).$$

It follows that

$$p_{\mathbf{X}_1 | \mathbf{X}_0}(x, y) \propto e^{-\frac{1}{2\sigma_1^2}(y - e^{-\alpha}x)^2}.$$

Combining these calculations, we conclude that the joint distribution has PDF given by

$$p^0(x, y) \propto e^{-\frac{1}{2}((1 + \sigma_1^{-2}e^{-2\alpha})x^2 - 2\sigma_1^{-2}e^{-\alpha}xy + \sigma_1^{-2}y^2)}.$$

This distribution is evidently a Gaussian with zero mean and covariance matrix Σ^0 given by

$$\Sigma^0 = \begin{pmatrix} \mathbf{I} & e^{-\alpha}\mathbf{I} \\ e^{-\alpha}\mathbf{I} & (\sigma_1^2 + e^{-2\alpha})\mathbf{I} \end{pmatrix}.$$

Note in particular that the variance of the marginal of π^0 at $t = 1$ is equal to the coefficient of the bottom-right entry of Σ^0 , which is $\sigma_1^2 + e^{-2\alpha}$. Now, the KL divergence between a 2-dimensional Gaussian distribution $\tilde{\pi}$ with zero mean and covariance matrix $\tilde{\Sigma}$ and the distribution π^0 is given explicitly by

$$D_{\text{KL}}(\tilde{\pi} \| \pi^0) = \frac{1}{2} \left(\log \frac{\det \Sigma^0}{\det \tilde{\Sigma}} - d + \text{Tr}(\Sigma^{0-1} \tilde{\Sigma}) \right).$$

If we take $\tilde{\Sigma}$ to be of the form

$$\tilde{\Sigma} = \begin{pmatrix} \mathbf{I} & S \\ S^T & \mathbf{I} \end{pmatrix},$$

which matches the form of the covariance Σ for π^* , then

$$D_{\text{KL}}(\tilde{\pi} \| \pi^0) = \frac{1}{2} \left(-\log \det \tilde{\Sigma} - 2e^{-\alpha}\sigma_1^{-2} \text{Tr}(S) + C \right)$$

where $C \in \mathbb{R}$ is a nonzero constant independent of $\tilde{\Sigma}$. As argued in the proof of Proposition 46 of De Bortoli et al. [2021], we can assume $S = S^T$ is a symmetric matrix, as doing so will only decrease $D_{\text{KL}}(\tilde{\pi} \| \pi^0)$, so S is diagonalizable. Let $\lambda_1, \dots, \lambda_d$ denote the eigenvalues of S , counted with multiplicity. Using the well-known formula for the determinant of a block 2×2 matrix, we find that

$$\det \tilde{\Sigma} = \det(\mathbf{I} - S^2) = \prod_{i=1}^d (1 - \lambda_i^2).$$

Thus, we obtain

$$D_{\text{KL}}(\tilde{\pi} \| \pi^0) = \frac{1}{2} \sum_{i=1}^d f(\lambda_i) + C, \quad \text{where} \quad f(x) = -\log(1 - x^2) - 2e^{-\alpha}\sigma_1^{-2}x.$$

Note in particular that since $\tilde{\Sigma}$ is a covariance matrix, it is positive semi-definite, and so its eigenvalues $1 - \lambda_i^2$ must be nonnegative, implying that $|\lambda_i| \leq 1$ for each i .

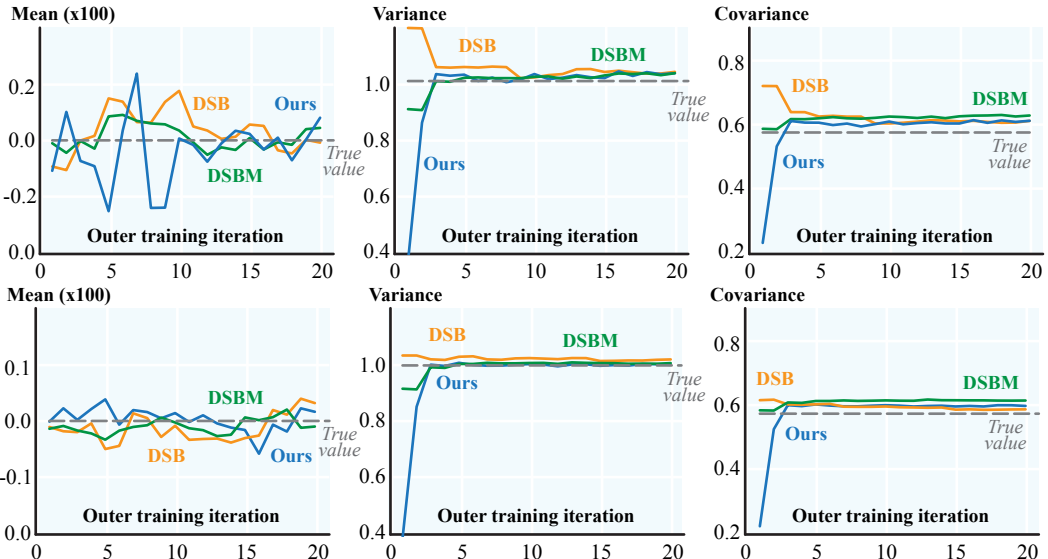


Figure 6: For each method, we plot the mean (left) and variance (middle) obtained for the terminal samples, i.e. samples obtained at time $t = T$, as well as the covariance (right) of the joint distribution, versus the number of outer iterations, averaged over 5 trials. Top: $d = 5$. Bottom: $d = 20$.

Minimizing $D_{\text{KL}}(\tilde{\pi} \parallel \pi^0)$ then amounts to take $\lambda_1 = \dots = \lambda_d = \beta$ in such a way that $f(\beta)$ is minimized. Observe that the equation

$$f'(\beta) = \frac{2\beta}{1 - \beta^2} - 2e^{-\alpha}\sigma_1^{-2} = 0$$

is solved by

$$\beta = \frac{\sigma^2(1 - e^{2\alpha}) \pm \sqrt{16e^{2\alpha}\alpha^2 + \sigma^4(1 - e^{2\alpha})^2}}{4\alpha e^\alpha}.$$

We then choose the sign to be $+$ to ensure that $|\beta| \leq 1$. \square

E Implementation Details

In this section we give further details on our experimental setup. Akin to Song and Ermon [2020, Technique 5] and De Bortoli et al. [2021, Technique 6], we improve performance of Algorithm 1 by implementing the exponential moving average (EMA) of network parameters. We run our experiments on a NVIDIA GeForce RTX 3090 GPU with 24GB of memory.

E.1 Gaussian Transport

We use the MLP large network from [De Bortoli et al., 2021] for DSB and DSBM in all Gaussian transport experiments. For our method, we modify this network to take σ as an input. The values of σ are uniformly sampled from the (inclusive) interval from 1 to 5 for training, and at test time we fix $\sigma = 1$ for all samples to compare with DSB and DSBM, which do not take σ as a network input, but each use $\sigma = 1$ via the SDE discretization. We run the same experiment for dimension $d = 5$ and $d = 20$ (in Fig. 6), and $d = 50$ (in Fig. 2). The number of samples for all experiments is 10,000. We use 20 timesteps and train for 10,000 inner iterations for each of 20 outer iterations.

E.2 2D Datasets

We modify the network architecture with positional encoding from [Vaswani et al., 2017], which is used by De Bortoli et al. [2021], to take values of noise σ rather than tuples of only \mathbf{X} and t . The values of σ are concatenated to the spatial features before the first MLP block is applied. This modified network is used to parametrize our drift function. We use Adam optimizer with learning rate 10^{-4} and momentum 0.9. We train each example for 10,000 inner iterations per outer iteration of the algorithm. Fig. 3 shows the terminal samples obtained for outer iteration 30 for all example datasets. The noise values σ^j are sampled uniformly in the range from 1 to 9 for training. At test time, a fixed

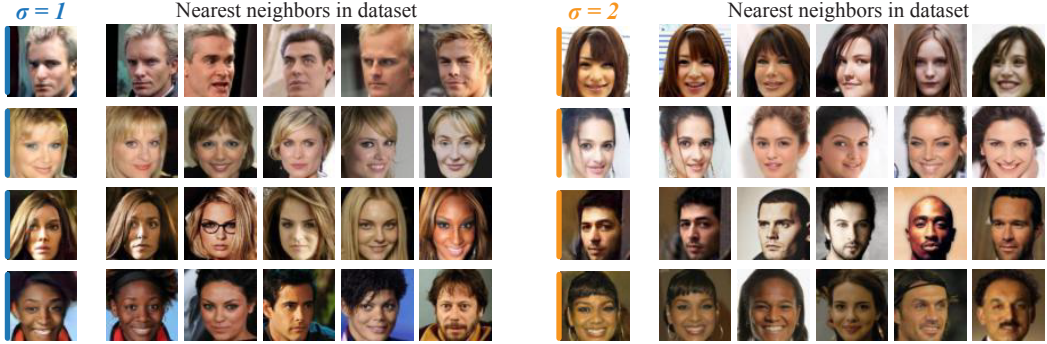


Figure 7: For our generated results (first and seventh columns), we show the five nearest neighbors in the CelebA dataset as measured through the features extracted by ResNet50 [He et al., 2016].

σ value is chosen for all sample trajectories. We train with 10,000 samples, which are refreshed each 1,000 iterations. We use 20 timesteps of size 0.01 each. All 2-dimensional experiments run on CPU.

E.3 Image Resampling

For the image dataset experiments, we modify the U-Net architecture used in [De Bortoli et al., 2021, Shi et al., 2023] to take values of noise σ . Each value σ^j is expanded to match image size and concatenated to channels of their corresponding sample image j before the input block is applied. For all image experiments we follow the timestep γ schedule used in De Bortoli et al. [2021] with $\gamma_{\min} = 10^{-5}$ and $\gamma_{\max} = 0.1$. We use Adam optimizer with learning rate 10^{-4} and momentum 0.9. Experiments with image datasets were run on limited shared GPU resources; lower-resolution image sizes and number of samples in cache were chosen accordingly.

MNIST. For the experiment in Fig. 4, we use 10,000 cached images of size 28×28 ; the batch size is 128 and the number of timesteps is 30. The noise values are sampled uniformly in the interval from 1 to 5 (inclusive) during training. We train for 5,000 iterations per outer iterations, and cached samples are refreshed every 1,000 inner iterations. The terminal samples shown are for outer iteration 8.

CelebA. In Fig. 5 and 12, we use 300 cached images of size 64×64 and batch size 128. The cache is refreshed every 100 inner iterations and we train for 5,000 iterations per outer iterations. The number of timesteps is 50; the σ values are uniformly sampled in the interval from 1 to 3. The terminal sample images are shown for outer iteration 15. The FID score in Fig. 5 is computed using 300 images.

F Additional Experimental Results

F.1 Control Over Sample Proximity

We define proximity of samples using pixel-wise L_2 norm as our choice of distance metric. In Fig. 8 (left), we demonstrate how larger values of σ effectively produce pushforward samples that are farther in this distance metric, compared to samples generated with smaller values of σ . This experiment expands the results shown in Fig. 3 to the case of resampling from image distributions. In particular, the mean and spread of the histograms in Fig. 8 (right) show that larger values of sigma correspond to higher average distance values relative to the initial sample, as well as greater variation among these distances.

F.2 Sample Path Regularity

We present empirical results on the regularity of path measures produced by our method. Specifically, in Fig. 8 (right), we give a histogram for the values of a metric defined by taking the ratio of total displacement to total path length for different values of σ . For a given sample trajectory $\{\mathbf{X}_i\}_{i=0}^{M-1}$, this metric is explicitly computed by dividing $\|\mathbf{X}_0 - \mathbf{X}_{M-1}\|_2$ (total displacement) and $\sum_k \|\mathbf{X}_{k+1} - \mathbf{X}_k\|_2$ (total path length). The greater the value of this metric, the greater the variation

in the trajectory; hence, smaller values of this metric are suggestive of greater sample path regularity. We find, as expected, that sample path regularity decreases as σ increases.

F.3 Integrity of Initial Distribution

We compute Chamfer distances as a means of measuring the proximity of the pushforward distributions exhibited in Fig. 3 to the corresponding initial distributions. In the mirror case, the pushforward distribution should match the initial distribution, and the Chamfer distance between them should therefore decay as the number of iterations grows. In Fig. 9, we demonstrate how the Chamfer distance decays over outer iterations of our method for the same 2D distribution with different values of σ (left), as well as how the Chamfer distance decays for different datasets with fixed σ value (right).

F.4 Comparison to Alternative Methods

We compare our method with DSB and DSBM for image resampling with the MNIST dataset as the initial and final marginal distribution. For this experiment, we use the implementation for DSB and DSBM-IPF available in the code repository for Shi et al. [2023]. We implement our algorithm based on the architecture provided, only modifying the model to take on σ as an input parameter for our method. We test all three methods with the same set of training parameters as described in Appendix E.3. We train our model with $\sigma = 1$ fixed to match the noise value in the SDE for the other two methods, which do not take σ as a model input.

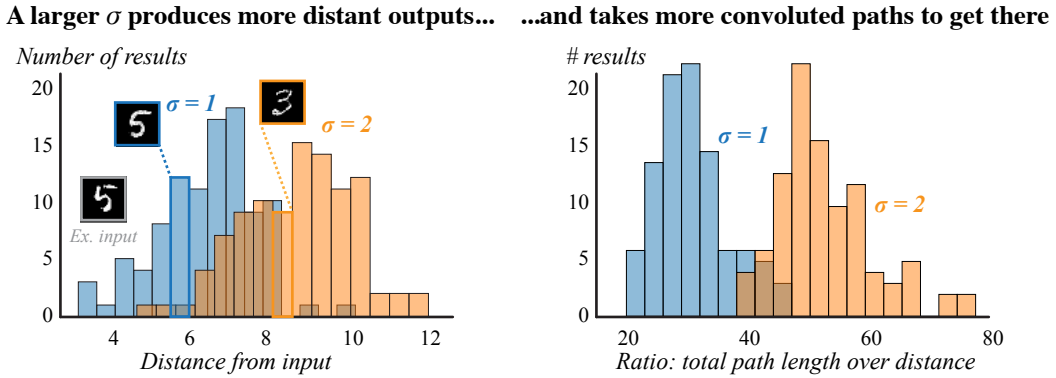


Figure 8: On the left: Two histograms demonstrating how image samples generated with larger σ correspond to less proximal samples relative to the initial image sample. On the right: Two histograms show the inverse ratio between displacement and total path length of sample paths as a metric of path regularity.

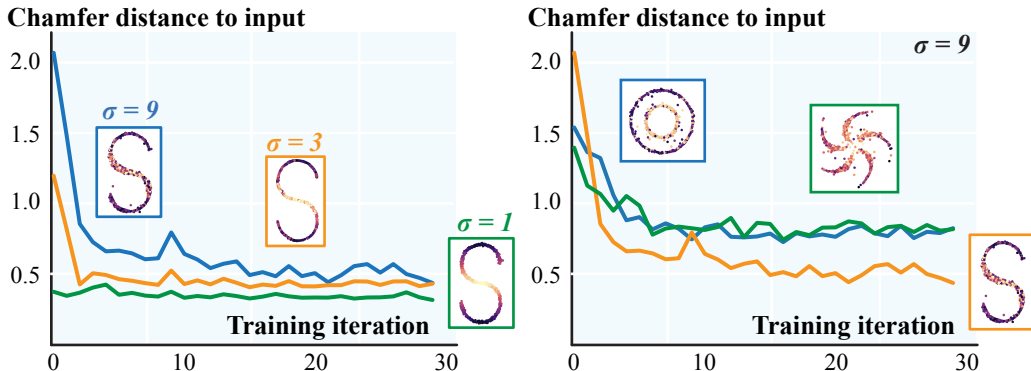


Figure 9: On the left: Three curves, each corresponding to a different σ value, showing convergence using Chamfer distance for the same 2D dataset (shown in Fig. 3). On the right: Three curves, each corresponding to a different 2D dataset, showing convergence for a fixed σ value.

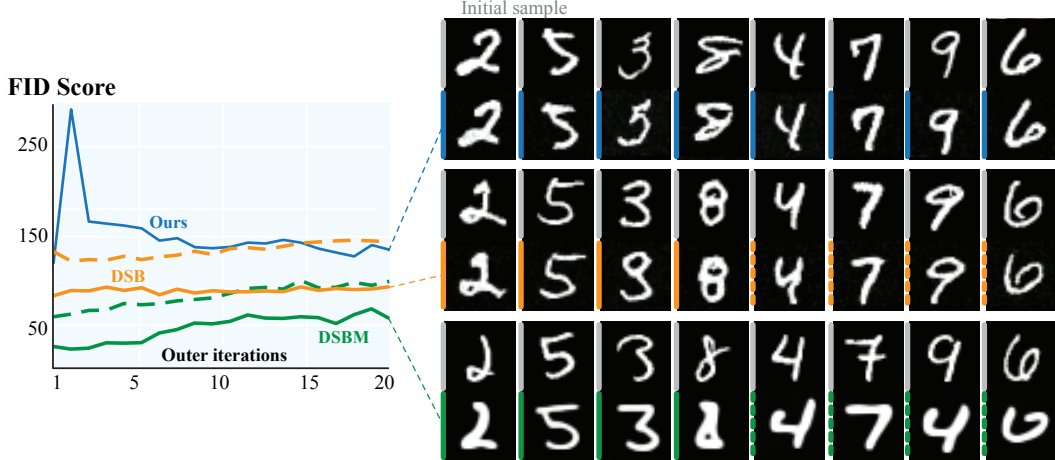


Figure 10: On the left: FID scores of pushforward samples versus outer iterations (single run) produced by our method, by DSB, and by DSBM, for a mirror bridge with the MNIST dataset as the marginal distribution. Solid lines correspond to backward models and dashed lines to forward models. On the right: Result of image resampling at outer iteration 20. For each method and drift direction, the initial samples are displayed on the upper row and the pushforward samples on the lower.

Table 1: Average runtimes for the experiment in Fig. 10

	Ours	DSB	DSBM-IPF	
Total	2.64	5.25	12.47	<i>hrs</i>
Outer Iter.	7.94	15.7	37.41	<i>min</i>
Inner Iter.	0.059	0.055	0.209	<i>s</i>
Inference	2.009	1.554	1.002	<i>s</i>

We provide FID scores for each method in Fig. 10. We observe that for DSB and DSBM, the forward and backward models result in pushforward samples of different quality. In particular, sample quality for the forward model is significantly lower than that of the backward. This indicates that neither of these methods converge to the mirror Schrödinger bridge for the given number of iterations, because the drift function for this bridge is necessarily time-symmetric, i.e., the forward and backward drifts must be equal to each other. In contrast, our algorithm provides time-symmetry by construction: a single model is trained and forcibly “symmetrized” at each outer iteration via the drift averaging procedure described in §4.3.

Also in Fig. 10, we present a breakdown of runtime for each method obtained for the same experiment. Our method has significantly lower total runtime and average outer training iteration time. The latter is not surprising, considering that one of the key features of our algorithm is to eliminate training for one of the projection steps taken; recall that we perform the reverse D_{KL} projection completely analytically. We observe that the average inference time during training, however, is higher with our method. Overall, in this particular experiment, we see that our method makes a trade-off between a small reduction in sample quality for a significant speed-up in training, while also preserving the time-symmetry of the solution.

E.5 Additional MNIST Results

Initial sample	$\sigma = 1$	$\sigma = 3$
1 5 5 4 3 3 3 0 8 3	1 5 0 4 3 8 3 0 8 3	1 3 3 9 3 5 5 4 8 1
2 4 3 8 2 1 3 9 8 8	2 4 3 8 2 1 3 9 8 8	3 9 3 7 6 1 3 1 9 6
6 0 7 0 8 9 9 8 5 5	0 0 7 0 0 9 9 8 5 8	4 6 7 0 8 5 9 3 2 5
7 9 2 2 5 3 3 2 6 2	2 9 2 2 5 3 9 2 6 2	3 7 4 2 1 0 5 2 6 2
6 6 1 3 1 0 0 9 3 5	6 6 1 3 2 0 0 9 8 5	2 6 1 0 2 2 0 8 9 9
4 2 3 6 3 3 0 0 8 2	1 2 3 6 8 3 0 0 8 2	6 7 3 6 8 9 5 6 5 2
9 7 4 8 2 6 9 7 2 9	9 2 4 8 2 6 2 7 2 4	4 7 4 5 3 6 4 1 1 9
7 2 1 2 4 9 0 6 9 7	7 2 1 2 9 4 0 6 7 7	4 1 8 8 3 8 8 4 1 6
8 3 5 6 8 8 8 6 0 9	1 8 5 6 8 8 9 6 0 9	0 5 3 7 7 8 1 4 0 5
9 0 0 7 0 1 6 5 7 8	9 8 0 7 0 1 6 5 7 8	8 5 7 7 0 1 2 5 6 8

Figure 11: Additional results for the empirical distribution of handwritten digits from which the examples in Fig. 4 are obtained.

E.6 Additional CelebA Results



Figure 12: Additional results for the empirical distribution of images in CelebA from which the examples in Fig. 5 are obtained.